*Computers, Materials & Continua*
DOI: 10.32604/cmc.2022.031976
***Article***

Tech Science Press

# Metaheuristic with Deep Learning Enabled Biomedical Bone Age Assessment and Classification Model

**Mesfer Al Duhayyim[1,*], Areej A. Malibari[2], Marwa Obayya[3], Mohamed K. Nour[4], Ahmed S. Salama[5], Mohamed I. Eldesouki[6], Abu Sarwar Zamani[7] and Mohammed Rizwanullah[7]**

[1]Department of Computer Science, College of Sciences and Humanities-Aflaj, Prince Sattam bin Abdulaziz University, Saudi Arabia
[2]Department of Industrial and Systems Engineering, College of Engineering, Princess Nourah bint Abdulrahman University, P.O. Box 84428, Riyadh, 11671, Saudi Arabia
[3]Department of Biomedical Engineering, College of Engineering, Princess Nourah bint Abdulrahman University, P.O. Box 84428, Riyadh, 11671, Saudi Arabia
[4]Department of Computer Sciences, College of Computing and Information System, Umm Al-Qura University, Saudi Arabia
[5]Department of Electrical Engineering, Faculty of Engineering & Technology, Future University in Egypt, New Cairo, 11845, Egypt
[6]Department of Information System, College of Computer Engineering and Sciences, Prince Sattam bin Abdulaziz University, AlKharj, Saudi Arabia
[7]Department of Computer and Self Development, Preparatory Year Deanship, Prince Sattam bin Abdulaziz University, AlKharj, Saudi Arabia
*Corresponding Author: Mesfer Al Duhayyim. Email: m.alduhayyim@psau.edu.sa
Received: 02 May 2022; Accepted: 06 June 2022

**Abstract:** The skeletal bone age assessment (BAA) was extremely implemented in development prediction and auxiliary analysis of medicinal issues. X-ray images of hands were detected from the estimation of bone age, whereas the ossification centers of epiphysis and carpal bones are important regions. The typical skeletal BAA approaches remove these regions for predicting the bone age, however, few of them attain suitable efficacy or accuracy. Automatic BAA techniques with deep learning (DL) methods are reached the leading efficiency on manual and typical approaches. Therefore, this study introduces an intellectual skeletal bone age assessment and classification with the use of metaheuristic with deep learning (ISBAAC-MDL) model. The presented ISBAAC-MDL technique majorly focuses on the identification of bone age prediction and classification process. To attain this, the presented ISBAAC-MDL model derives a mask Region-related Convolutional Neural Network (Mask-RCNN) with MobileNet as baseline model to extract features. Followed by, the whale optimization algorithm (WOA) is implemented for hyperparameter tuning of the MobileNet method. At last, Deep Feed-Forward Module (DFFM) based age prediction and Radial Basis Function Neural Network (RBFNN) based stage classification approach is utilized. The experimental evaluation of the ISBAAC-MDL model is tested using benchmark dataset and the outcomes are assessed over distinct factors. The

This work is licensed under a Creative Commons Attribution 4.0 International License, which permits unrestricted use, distribution, and reproduction in any medium, provided the original work is properly cited.

experimental outcomes reported the better performances of the ISBAAC-MDL model over recent approaches with maximum accuracy of 0.9920.

**Keywords:** Biomedical images; bone age assessment; age prediction; computer vision; deep learning; image classification

## 1 Introduction

The progression in healthcare technologies presents highly effective e-health care structures to the healthcare sector benefitting the medical specialists for good medications for patients. E-health care structures has been helpful in numerous medicinal fields [1]. But many computer visualization related biomedical imaging applications obtained high significance due to such applications offering detectable info to the radiotherapists for superior medication. Skeletal bone age assessment (BAA) is an algorithm which can be utilized for therapeutic inquiry and analytic of endocrinology difficulties like children's growth and genetic disorders, in the domain of pediatric radiology [2]. The BAA methodology is usually accomplished by radiological scrutiny of the left hand, because the peculiar character of bone ossification levels of the non-dominant hand, and after which comparison done with chronological ages. In reality, the radiotherapists usually adjust the bone age through witnessing the X-ray pictures of the non-dominant hand of subject [3,4]. They get more interest in the adulthood extent of the wrist bones, metacarpal bones, and the lowest termination of the ulna for predicting skeletal bone age which has been extensively termed as the regions of interest (RoIs) in BAA methods. Even though labor-intensive methodologies were widely implied in medical training, these old methodologies mostly depend on the radiologist's experience, that leads to the truth that the proficiency could not be ensured and the analysis outcome differs every time among distinct radiotherapists [5].

Many image processing systems were utilized for BAA [6]. Separation is the first and foremost stage in image processing application areas which abstract the ROIs from diverse image modes namely MRI, X-rays, and CT scans [7]. Segmentation of ROIs is regarded as significant job for BAA. X-ray and MRI has different characteristics which have been employed for BAA which adds structure tensor eigenvalues, local histograms, and image textures [8]. Deep learning (DL) has grabbed more interest in medical imaging difficulties. Lately, encouraged by the triumph of deep convolutional neural network system (DCNN) in image categorization [9], research works in medical imaging were exploring these approaches. DL-related methodologies permit neglecting feature engineering through mechanically studying the order of discriminate features right from a set of drill information. DCNN was effectively used in the BAA [10]. These methodologies suggest an endwise learning architectures to guesstimate bone age by employing DCNN.

In [11], the researchers presented a DL based technique to BAA with integration of Tanner-Whitehouse (TW3) approaches and deep convolutional network system dependent upon extracting regions of interest (ROI) recognition and classifier employing Faster-RCNN and Inception-v4 network correspondingly. The presented approach permits the investigation of expert data in the TW3 and feature engineering in deep convolutional network for enhancing the accuracy of BAA. Son et al. [12] presented a whole end-to-end BAA technique for automating the total procedure of TW3 approach, beginning from localization of epiphysis metaphysis development areas in 13 distinct bones and finishing with estimate of equivalent BA. The particular alterations to CNNs and other phases were presented for improving outcomes. Also, the annotated databases of 3300 X-ray images was constructed for training and evaluating the method.

Tong et al. [13] progress a deep automated skeletal BAA method dependent upon CNNs and support vector regression (SVR) utilizing multiple kernel learning (MKL) technique for processing heterogeneous structures. In [14], the authors assumed that important region and present a novel deep automated skeletal BAA technique using region-related CNN (R-CNN). The Faster R-CNN (Faster R-CNN) technique was executed in object detection for bone age regression to identify the ossification centers of epiphysis and carpal bone and estimate bone age. The presented technique overcomes the restriction of other CNN related techniques, obtaining large-scale original X-ray images as input. In [15–19], the authors presented a novel DL based techniques for improving the BAA trained from both training and pre-training structures. In the pre training structure, it can be presented a structure utilizing a novel distance metric of cosine distance from the structure of optimum carrying for data augmentation (CNN-GAN-OTD). During the training structure, it can be discovered the procedure of bone age and gender label data, semi-supervised and supervised training.

This article introduces an intellectual skeletal bone age assessment and classification with the help of metaheuristic with deep learning (ISBAAC-MDL) approach. The presented ISBAAC-MDL technique derives a mask Region-related Convolutional Neural Network (Mask-RCNN) with MobileNet as baseline model to extract features. Followed by, the whale optimization algorithm (WOA) was implemented for hyperparameter tuning of the MobileNet model. At last, Deep Feed-Forward Module (DFFM) based age prediction and Radial Basis Function Neural Network (RBFNN) based stage classification technique is utilized. The experimental evaluation of the ISBAAC-MDL model is tested using benchmark dataset and the outcomes are assessed over distinct prospects.

The rest of the paper is organized as follows. Section 2 offers the proposed model and the Section 3 provides the experimental validation. Lastly, Section 4 concludes the work.

## 2 The Proposed BAA Model

In this article, a novel ISBAAC-MDL method was enhanced for the effective bone age prediction and classification process. Initially, the Mask-RCNN with MobileNet as baseline model is utilized to extract features. Then, the WOA was implemented for hyperparameter tuning of the MobileNet technique. Next, the DFFM based age prediction and RBFNN based stage classification model is utilized.

### *2.1 Module I: Feature Extraction Process*

Primarily, the Mask-RCNN with MobileNet as baseline model is utilized to extract features. In the Mask R-CNN is an effectual DL framework that combines the semantic segmentation and object detection procedure. It mostly contains 2 levels of functions such as generating region proposals and categorizing every generated proposal [20]. An input X-ray image was primarily got into a convolutional networks termed a backbone networks and its influence obtain varies dependent upon the needed trade-off amongst the efficiency, trained speed, and restricted due to the computation power. During the Mask R-CNN method, the MobileNet structure was utilized as the baseline method. MobileNet is a CNN based methodology that can be extensively used for the classification mechanism. The great benefits of the use of MobileNet model are that they need lower computation power compared to the standard CNN technique, making them fit to operate with mobile gadgets and the computer that operates with less computation capability. The MobileNet was considered as a fundamental architecture that incorporates convolution layers that are applied in discriminating the information on the basis of two controllable characteristics that switches among the parameter's latency and accuracy. The MobileNet architecture is benefited in minimizing the size of the

network [21]. MobileNet architecture is effective correspondingly with an insignificant quantity of features, namely Palmprint Detection. The difficulty of $1 \times 1$ is termed as a pointwise difficulty Platforms to make in-depth were designed to have points via an average, ReLU, and abstract layer with in-depth structure. Fig. 1 depicts the process of Mask RCNN technique.

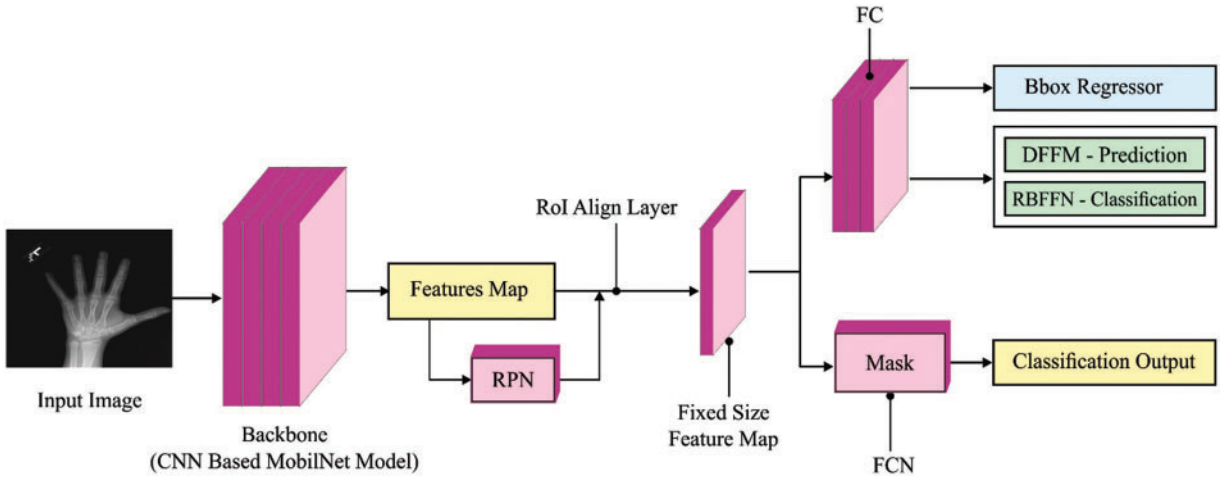


**Figure 1:** Process of Mask RCNN Model

Where filter is of size is represented as $F_s \times F_s$ and vector feature mapping of size is indicated by $F_m \times F_m$, the output variable is called $q$, and the input variable is characterized by $p$. For the abstraction layer, the computation effort is considered a variable $c_e$ and it is evaluated as follows:

$$c_e = F_s \cdot F_s \cdot \omega \cdot \alpha F_m \cdot \alpha F_m + \omega \cdot \rho \cdot \alpha F_m \cdot \alpha F_m \tag{1}$$

The value of resolution multipliers known as $\alpha$ is deliberated to be one. The values of multiplier $\omega$ lie within the range of $[1, n]$. The variable $cost_e$ is evaluated as follows:

$$cost_e = F_s \cdot F_s \cdot \omega \cdot \rho \cdot F_m \cdot F_m \tag{2}$$

The proposed methodology combines the pointwise and depthwise convolution are constrained by the reduction variable represented as $d$ parameter and it is evaluated as follows:

$$d = \frac{F_s \cdot F_s \cdot \omega \cdot \alpha F_m \cdot \alpha F_m + \omega. \cdot \rho \cdot \alpha F_m \cdot \alpha F_m}{F_s \cdot F_s \cdot \omega \cdot \rho \cdot F_m F_m} \tag{3}$$

The two hyper features, such as the resolution and width multipliers help to modify the optimal size window for predicting accurately. The third values recommend that it has three input networks. The given architecture comprises the filter size is $3 \times 3 \times 3 \times 32$, and thirty-two filters.

The principle under the MobileNet framework replaces complex convolutional layer in which every single layer involves a convolutional layers of size $3 \times 3$ that buffers the input dataset, along with a convolution layer of size $1 \times 1$ pointwise which combines the filtered variable for constructing a novel element. The abovementioned concept illustrates the technique and makes them faster when compared to the standard convolutional process. The residual and downsizing layers encompass three sub-layers.

### *2.2 Module II: Hyperparameter Optimization*

At this stage, the WOA was implemented for hyperparameter tuning [22–24] of the MobileNet system. The WOA has been executed. Firstly, an initialization process takes place. In the neighboring prey method, the humpback whales are distinguished that the position of prey and surrounded them [25]. For uncertain locations in the searching region, the present optimal outcome was considered by prey. When tan optimal search agent was defined, another searching space revives the criteria in the optimal searching region.

$$\vec{\mathrm{U}} = \left| S.\vec{K}^{*}(t) - \vec{K}(t) \right| \tag{4}$$

$$\vec{\mathrm{K}}(\mathrm{t}+1) = .\vec{K}^{*}(\mathrm{t}_{\mathrm{best}}) - \mathrm{Y}^{*}\vec{\mathrm{U}}.$$

In Eq. (4), $\mathrm{S} = 2.\mathrm{r}$ and $\mathrm{Y} = 2.\mathrm{I}.r - \mathrm{I}$. A newly accomplished outcome for optimal fitness is associated with the highlight that composes certain variable dependence. It couldn't need to define the major set of variables and step size to ideal solution.

According to the fitness value of the abovementioned iterations, the "$y$" coefficient vector is achieved by getting the possible probability operation as:

$$\mathrm{y} \Rightarrow \mathit{Probability} = \begin{cases} \mathrm{C}_1 \left(\mathrm{f}_{\max} - \mathrm{f}_{\mathrm{x}}\right) / \left(\mathrm{f}_{\max} - \mathrm{F}_{\mathrm{avg}}\right), & \mathrm{f}_{\mathrm{x}} \geq \mathrm{F}_{\mathrm{avg}} \\ \mathrm{C}_3, & \mathrm{f}_{\mathrm{x}} \leq \mathrm{f}_{\mathrm{avg}}. \end{cases} \tag{5}$$

In Eq. (5), $\mathrm{f}_{\min}$ and $\mathrm{f}_{\max}$ indicates the least and highest value of fitness function, however, $\mathrm{C}_1$ and $\mathrm{C}_3$ range within [0,1]. The position of ideal solution was transformed vigorously by fitness function. Next, for defining the bubble-net nature of humpback whales, 2 improved methodologies are applied. The bubble-net procedure takes place using exploitation along with exploration stages.

The spiral process was implemented among the location of whale and prey to imitate the helix-framed growth of humpback whale that is represented by following equation:

$$\vec{\mathrm{K}}(\mathrm{t}+1) = \mathrm{e}^{bt}.\cos(2\pi.\mathrm{y}).\vec{\mathrm{U}}' + \vec{K}^{*}(t). \tag{6}$$

It has been noted that the humpback whale swims through the prey in the contracting circle and winding molded methodology.

In order to illustrate the synchronous efficacy, the probability of fifty percentage has forecasted for choosing the constricting spiral and enclosed system for refreshing the whale condition. It can be mathematically formulated in the subsequent equation:

$$\vec{\mathrm{K}}(\mathrm{t}+1) = \begin{cases} \vec{K}(\mathrm{t}) - y..\vec{U} & if \;\; p < 0.5 \\ \vec{\mathrm{U}}'.e^{bs}.\cos(2\pi s) + \vec{\mathrm{K}}(\mathrm{t}) & if \;\; p \geq 0.5, \end{cases} \tag{7}$$

In which $\mathrm{y} \rightarrow$uninformed distributed number ranges from [−1 to 1], demonstrate the synchronous efficacy specifically acceptable that there are possibilities of half for gathering between composed the contracting adjacent procedure and twisted procedure for refreshing the whale condition from center of optimization. The administrator's request has motivated by purposelessly selected searching agent beforehand a most favorable searching agent is found in the following equation:

$$\vec{\mathrm{U}} = \left| \vec{\mathrm{S}}.\overline{\mathrm{K}}_{rand} - \vec{\mathrm{K}} \right| \tag{8}$$

$$\mathrm{K}(\mathrm{t}+1) = \vec{\mathrm{K}}_{\mathrm{rand}} - \vec{\mathrm{Y}}.\vec{\mathrm{U}}. \tag{9}$$

Therefore, the uninformed distributed random number was applied essentially on 1 or under −1 to make searching experts move reserved in orientation whale. Next, in the exploitation stage, the position of searching agent has revitalized in the exploration process as declared by using subjectively-chosen searching agent beforehand an optimal searching agent demonstrating the point. This approach $|\vec{Y}| > 1$ highlights the exploration and considers the WOA technique for proceeding a global best searching and $|\vec{Y}| > 1$ for motivating the position of searching operator. This procedure is repeated until the greatest quantity of iterations gets accomplished. A novel set of solutions are authenticated and trailed according to the upgraded method.

### *2.3 Module III: DFFM Based Age Prediction*

In this study, the DFFM model receives the features and performs effective age prediction process [26]. In fully connected (FC) model, the neuron receives certain input, implements dot products, and utilizes non-linear functions namely ReLU, Tanh, Parametric ReLU, Sigmoid, Leaky ReLU, etc., allowing a model to create complex mapping among input and output of the networks. This is significant for datasets with higher dimensionality. All the neurons make use of a non-linear activation and the final layer makes use of softmax layer. During forward pass, a series of processes which convert input to output is implemented. Activation function is utilized for presenting nonlinear into the network and learning complex functions. The backward pass is utilized when a wrong output is obtained. In backpropagation, error gradient concerns neuron weight and bias are evaluated. Cross-entropy or log loss could evaluate the outcome of the classifier method with outputs among zero and one. The loss function might be a distinct mathematical expression. When $x \in R$ indicates the input to the FC layer, $y_i \in R$ represents the *i-th* outputs from the FC layer. Thus, $y_i \in R$ is calculated by:

$$y_i = \sigma\ (w_1 x_1 + w_2 x_2 + \ldots + w_m x_m) \tag{10}$$

The $\sigma$ non-linear function is a rectifier to resolve gradient vanishing problems:

$$\sigma = \max\ (0, x) \tag{11}$$

DFFM could be trained fast when compared to SRBMM. Thus, a deep network having twelve hidden layer is utilized. We utilize BN with batch size of 10000 rather than a dropout method for getting accurate outcomes and the gradient of complete data would have a stable estimation. The batch size changes the learning speed and doesn't affect the quality of learning. Also, In order to prevent this algorithm from memorizing the attack, earlier stopping is utilized. We employ the 0.01 value as the learning rate; selecting a small value might result in long training time and high value makes the training not stable. Adam optimization algorithm was regarded as an extension of stochastic gradient descent utilized to update the network weight, this model is very efficient when compared to RMSProp or AdaGrad. Cross entropy is utilized in multiple class scenarios. Fig. 2 illustrates the framework of DFFM.

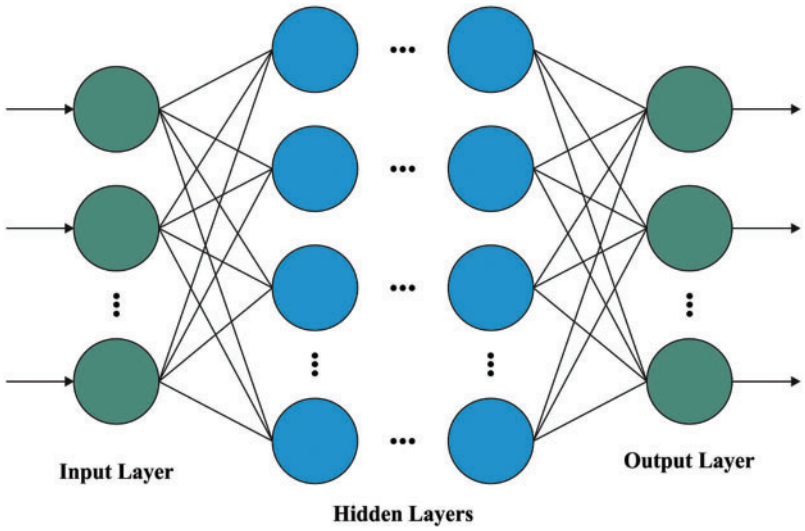


**Figure 2:** Structure of DFFM

### *2.4 Module IV: RBFNN Based Stage Classification*

At the same time, the RBFNN model is utilized for effective stage classification process. The RBFNN [27] is a multiple layer forward network that can able to approximate non-linear operation and avoid plunging into local minimal. Typically, the RBFNN comprises input and hidden layers with a linear output layer, and nonlinear RBF activation function. The input of RBFNN is a traffic vector dataset that is modeled by:

$$X_t = (x_{t-1}, x_{t-2}, \ldots, x_{t-g})^T \tag{12}$$

In Eq. (12), $x_t$ indicates preceding dataset and $g$ characterize the amount of input layers. The output of RBFNN is a scalar function of input vector that is given by:

$$Y(X_t) = \sum_{i=1}^{M} \omega_i \phi(X_t, c_i) \tag{13}$$

In Eq. (13) $M$ indicates the amount of layers in the hidden neuron; $\phi(X_t, c_i)$ denotes the radial basis function; $c_i$ represents the center vector for $i$ neuron; $\omega_i$ represent the neuron weight $i$ in the linear output neurons. In the structure of RBFNN, each input is interconnected to hidden neuron. Typically, the norm is considered as Euclidean distance, and the RBF is usually considered as the Gaussian that is formulated by

$$\phi(X_t, c_i) = \exp\left(-\frac{\|X_t - c_i\|^2}{2\sigma_i^2}\right) \tag{14}$$

In Eq. (14), $\sigma_i$ indicates the standardized constant of $i^{th}$ hidden unit that indicates the width of RBF nearby the center vector.

## 3 Results and Discussion

The performance validation of the ISBAAC-MDL technique is tested with existing models under distinct sizes of training size (TS) data and cross-validation (CV). A few sample images are illustrated

in Fig. 3, Tab. 1 and Fig. 4 provide detailed maturity stage classification outcomes of the ISBAAC-MDL model with recent models under varying sizes of TS. The results indicated that the ISBAAC-MDL model has obtained effectual outcomes with maximum classification results under all TSs. For instance, with TS = 40%, the ISBAAC-MDL model has accomplished higher $sens_y$ of 0.9843 whereas the DL-BAAC, CNN-WELM, CNN-KELM, and CNN-ELM models have obtained lower $sens_y$ of 0.9789, 0.9778, 0.9833, and 0.9817 respectively. Also, with TS = 50%, the ISBAAC-MDL method has established higher $sens_y$ of 0.9962 whereas the DL-BAAC, CNN-WELM, CNN-KELM, and CNN-ELM algorithms have gained lower $sens_y$ of 0.9768, 0.9822, 0.9805, and 0.9831 correspondingly. Besides, with TS = 60%, the ISBAAC-MDL algorithm has accomplished higher $sens_y$ of 0.9687 whereas the DL-BAAC, CNN-WELM, CNN-KELM, and CNN-ELM systems have attained lower $sens_y$ of 0.9596, 0.9574, 0.9545, and 0.9563 correspondingly. Eventually , with TS = 70%, the ISBAAC-MDL model has presented higher $sens_y$ of 0.9994 whereas the DL-BAAC, CNN-WELM, CNN-KELM, and CNN-ELM models have attained lower $sens_y$ of 0.9913, 0.9940, 0.9863, and 0.9811 correspondingly. At last, with TS = 80%, the ISBAAC-MDL model has accomplished higher $sens_y$ of 0.9870 while the DL-BAAC, CNN-WELM, CNN-KELM, and CNN-ELM models have reached lower $sens_y$ of 0.9834, 0.9723, 0.9721, and 0.9739 correspondingly.

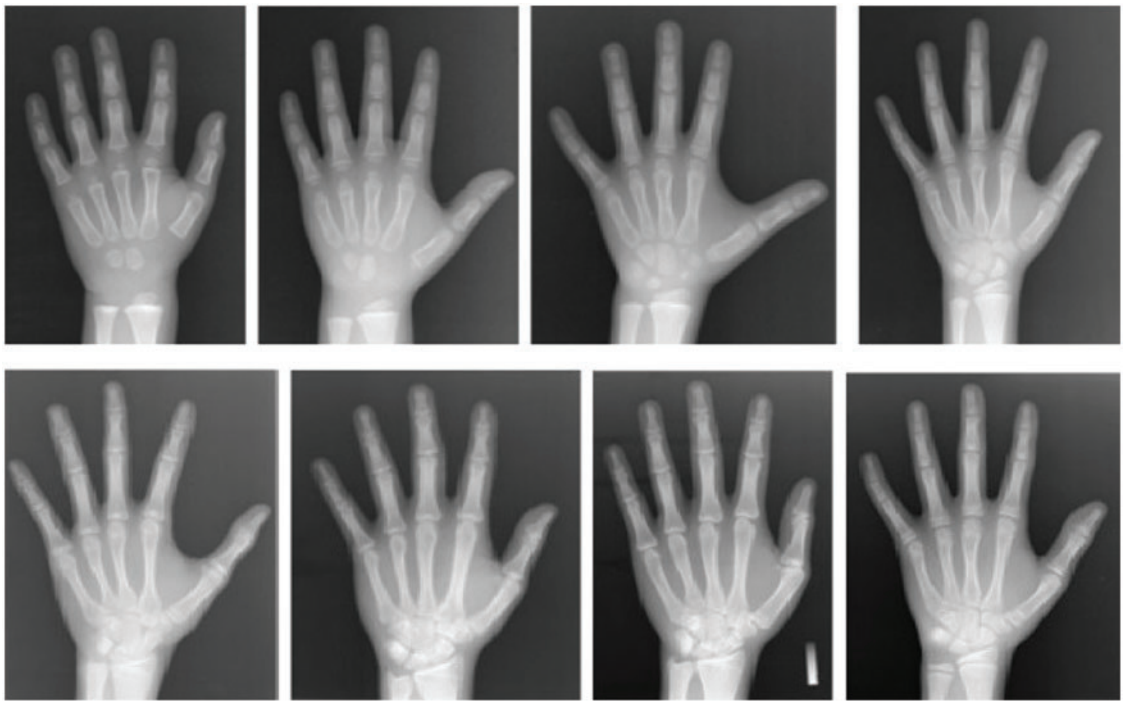

**Figure 3:** Sample bone images

**Table 1:** Maturity stage classification results of ISBAAC-MDL model with existing models under distinct TS

| Training size (%) | ISBAAC-MDL | DL-BAAC | CNN-WELM | CNN-KELM | CNN-ELM |
|---|---|---|---|---|---|
| | | | Sensitivity | | |
| TS = 40 | 0.9843 | 0.9789 | 0.9778 | 0.9833 | 0.9817 |
| TS = 50 | 0.9962 | 0.9768 | 0.9822 | 0.9805 | 0.9831 |
| TS = 60 | 0.9687 | 0.9596 | 0.9574 | 0.9545 | 0.9563 |
| TS = 70 | 0.9994 | 0.9913 | 0.9940 | 0.9863 | 0.9811 |
| TS = 80 | 0.9870 | 0.9834 | 0.9723 | 0.9721 | 0.9739 |
| Average | 0.9871 | 0.9780 | 0.9767 | 0.9753 | 0.9752 |
| | | | Specificity | | |
| TS = 40 | 0.9703 | 0.9697 | 0.9641 | 0.9607 | 0.9629 |
| TS = 50 | 0.9921 | 0.9841 | 0.9769 | 0.9758 | 0.9678 |
| TS = 60 | 0.9913 | 0.9754 | 0.9764 | 0.9664 | 0.9746 |
| TS = 70 | 0.9984 | 0.9752 | 0.9742 | 0.9834 | 0.971 |
| TS = 80 | 0.9688 | 0.9572 | 0.9583 | 0.9503 | 0.9581 |
| Average | 0.9842 | 0.9723 | 0.9700 | 0.9673 | 0.9669 |
| | | | Accuracy | | |
| TS = 40 | 0.9944 | 0.9859 | 0.9728 | 0.9754 | 0.9725 |
| TS = 50 | 0.9907 | 0.9884 | 0.9884 | 0.9885 | 0.9895 |
| TS = 60 | 0.9925 | 0.9841 | 0.9871 | 0.9831 | 0.9834 |
| TS = 70 | 0.9938 | 0.9711 | 0.9739 | 0.9628 | 0.9684 |
| TS = 80 | 0.9830 | 0.9707 | 0.9756 | 0.9808 | 0.9727 |
| Average | 0.9909 | 0.9800 | 0.9796 | 0.9781 | 0.9773 |
| | | | F-score | | |
| TS = 40 | 0.9934 | 0.9833 | 0.9792 | 0.9826 | 0.9713 |
| TS = 50 | 0.9900 | 0.9889 | 0.9780 | 0.9789 | 0.9825 |
| TS = 60 | 0.9972 | 0.9868 | 0.9788 | 0.9854 | 0.9877 |
| TS = 70 | 0.9800 | 0.9621 | 0.9736 | 0.9595 | 0.9644 |
| TS = 80 | 0.9939 | 0.9721 | 0.9817 | 0.9704 | 0.9672 |
| Average | 0.9909 | 0.9786 | 0.9783 | 0.9754 | 0.9746 |

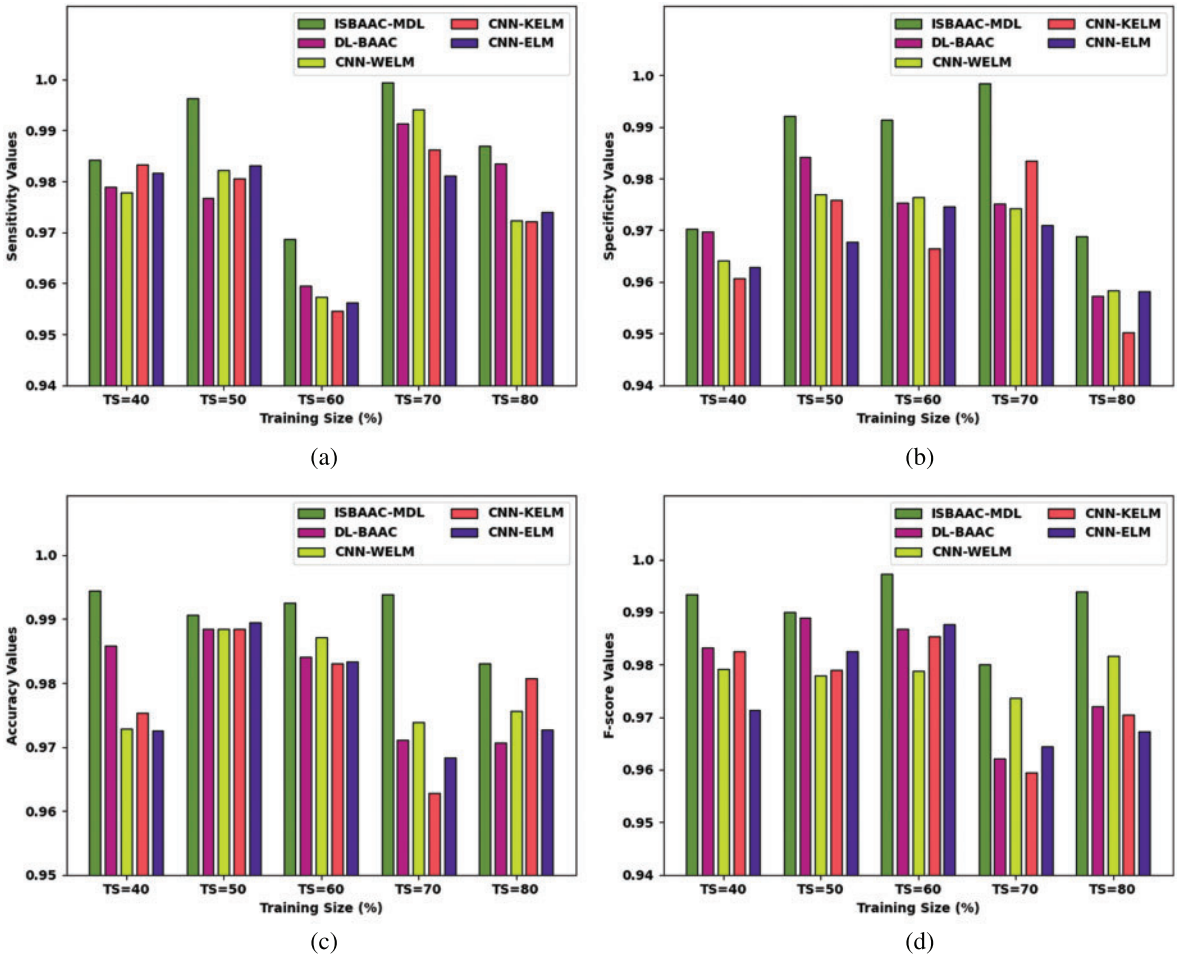


**Figure 4:** Result analysis of ISBAAC-MDL technique under distinct TS (a) $Sens_y$, (b) $Spec_y$, (c) $Accu_y$, and (d) $F_{score}$

Fig. 5 reports an average classifier outcome of the ISBAAC-MDL model with recent models. The figure inferred the enhanced performance of the ISBAAC-MDL model over other models. Concerning $sens_y$, the ISBAAC-MDL model has offered increased average $sens_y$ of 0.9871 whereas the DL-BAAC, CNN-WELM, CNN-KELM, and CNN-ELM models have provided decreased $sens_y$ of 0.9780, 0.9767, 0.9753, and 0.9752 respectively. Also, with respect to $accu_y$, the ISBAAC-MDL method has provided raised average $accu_y$ of 0.9909 whereas the DL-BAAC, CNN-WELM, CNN-KELM, and CNN-ELM techniques have offered reduced $accu_y$ of 0.9800, 0.9796, 0.9781, and 0.9773 correspondingly. Eventually, with respect to $F_{score}$, the ISBAAC-MDL algorithm has rendered increased average $F_{score}$ of 0.9909 while the DL-BAAC, CNN-WELM, CNN-KELM, and CNN-ELM models have offered reduced $F_{score}$ of 0.9786, 0.9783, 0.9754, and 0.9746 correspondingly.


**Figure 5:** Average analysis of ISBAAC-MDL technique under distinct TS (a) $Sens_y$, (b) $Spec_y$, (c) $Accu_y$, and (d) $F_{score}$

Tab. 2 and Fig. 6 present detailed maturity stage classification results of the ISBAAC-MDL model with current methods under varying sizes of CV. The outcomes indicated that the ISBAAC-MDL model has gained effectual outcomes with maximum classification results under all CVs. For example, with CV = 6, the ISBAAC-MDL model has accomplished higher $sens_y$ of 0.9993 whereas the DL-BAAC, CNN-WELM, CNN-KELM, and CNN-ELM models have gained lower $sens_y$ of 0.9849, 0.9931, 0.9864, and 0.9916 correspondingly. Additionally, with CV = 7, the ISBAAC-MDL model has established higher $sens_y$ of 0.9966 whereas the DL-BAAC, CNN-WELM, CNN-KELM, and CNN-ELM models have obtained lower $sens_y$ of 0.9901, 0.9874, 0.9767, and 0.9735 respectively. Also, with CV = 8, the ISBAAC-MDL algorithm has established higher $sens_y$ of 0.9983 whereas the DL-BAAC, CNN-WELM, CNN-KELM, and CNN-ELM models have reached lower $sens_y$ of 0.9681, 0.9633, 0.9653, and 0.9564 correspondingly. Meanwhile, with CV = 9, the ISBAAC-MDL technique has accomplished higher $sens_y$ of 0.9931 whereas the DL-BAAC, CNN-WELM, CNN-KELM, and CNN-ELM techniques have gained lower $sens_y$ of 0.9828, 0.9902, 0.9831, and 0.9860 correspondingly. Finally, with CV = 10, the ISBAAC-MDL model has established higher $sens_y$ of 0.9925 whereas the DL-BAAC, CNN-WELM, CNN-KELM, and CNN-ELM methodologies have obtained lower $sens_y$ of 0.9879, 0.9789, 0.9815, and 0.9798 correspondingly.

**Table 2:** Maturity Stage Classification results of ISBAAC-MDL model with existing models under distinct CV

| No. of cross validation | ISBAAC-MDL | DL-BAAC | CNN-WELM | CNN-KELM | CNN-ELM |
|---|---|---|---|---|---|
| | | | Sensitivity (%) | | |
| CV = 6 | 0.9993 | 0.9849 | 0.9931 | 0.9864 | 0.9916 |
| CV = 7 | 0.9966 | 0.9901 | 0.9874 | 0.9767 | 0.9735 |
| CV = 8 | 0.9983 | 0.9681 | 0.9633 | 0.9653 | 0.9564 |
| CV = 9 | 0.9931 | 0.9828 | 0.9902 | 0.9831 | 0.9860 |
| CV = 10 | 0.9925 | 0.9879 | 0.9789 | 0.9815 | 0.9798 |
| Average | 0.9960 | 0.9828 | 0.9826 | 0.9786 | 0.9775 |
| | | | Specificity (%) | | |
| CV = 6 | 0.9758 | 0.9670 | 0.9589 | 0.9644 | 0.9740 |
| CV = 7 | 0.9827 | 0.9792 | 0.9777 | 0.9768 | 0.9690 |
| CV = 8 | 0.9795 | 0.9736 | 0.9765 | 0.9760 | 0.9688 |
| CV = 9 | 0.9944 | 0.9770 | 0.9850 | 0.9838 | 0.9792 |
| CV = 10 | 0.9913 | 0.9697 | 0.9611 | 0.9558 | 0.9591 |
| Average | 0.9847 | 0.9733 | 0.9718 | 0.9714 | 0.9700 |
| | | | Accuracy (%) | | |
| CV = 6 | 0.9900 | 0.9841 | 0.9812 | 0.9706 | 0.9719 |
| CV = 7 | 0.9971 | 0.9800 | 0.9786 | 0.9923 | 0.9814 |
| CV = 8 | 0.9900 | 0.9832 | 0.9820 | 0.9732 | 0.9780 |
| CV = 9 | 0.9957 | 0.9729 | 0.9670 | 0.9625 | 0.9683 |
| CV = 10 | 0.9870 | 0.9786 | 0.9827 | 0.9754 | 0.9701 |
| Average | 0.9920 | 0.9798 | 0.9783 | 0.9748 | 0.9739 |
| | | | F-score (%) | | |
| CV = 6 | 0.9905 | 0.9804 | 0.9845 | 0.9735 | 0.9812 |
| CV = 7 | 0.9989 | 0.9894 | 0.9917 | 0.9903 | 0.9799 |
| CV = 8 | 0.9978 | 0.9832 | 0.9778 | 0.9830 | 0.9733 |
| CV = 9 | 0.9966 | 0.9740 | 0.9648 | 0.9627 | 0.9734 |
| CV = 10 | 0.9944 | 0.9825 | 0.9724 | 0.9757 | 0.9717 |
| Average | 0.9956 | 0.9819 | 0.9782 | 0.9770 | 0.9759 |

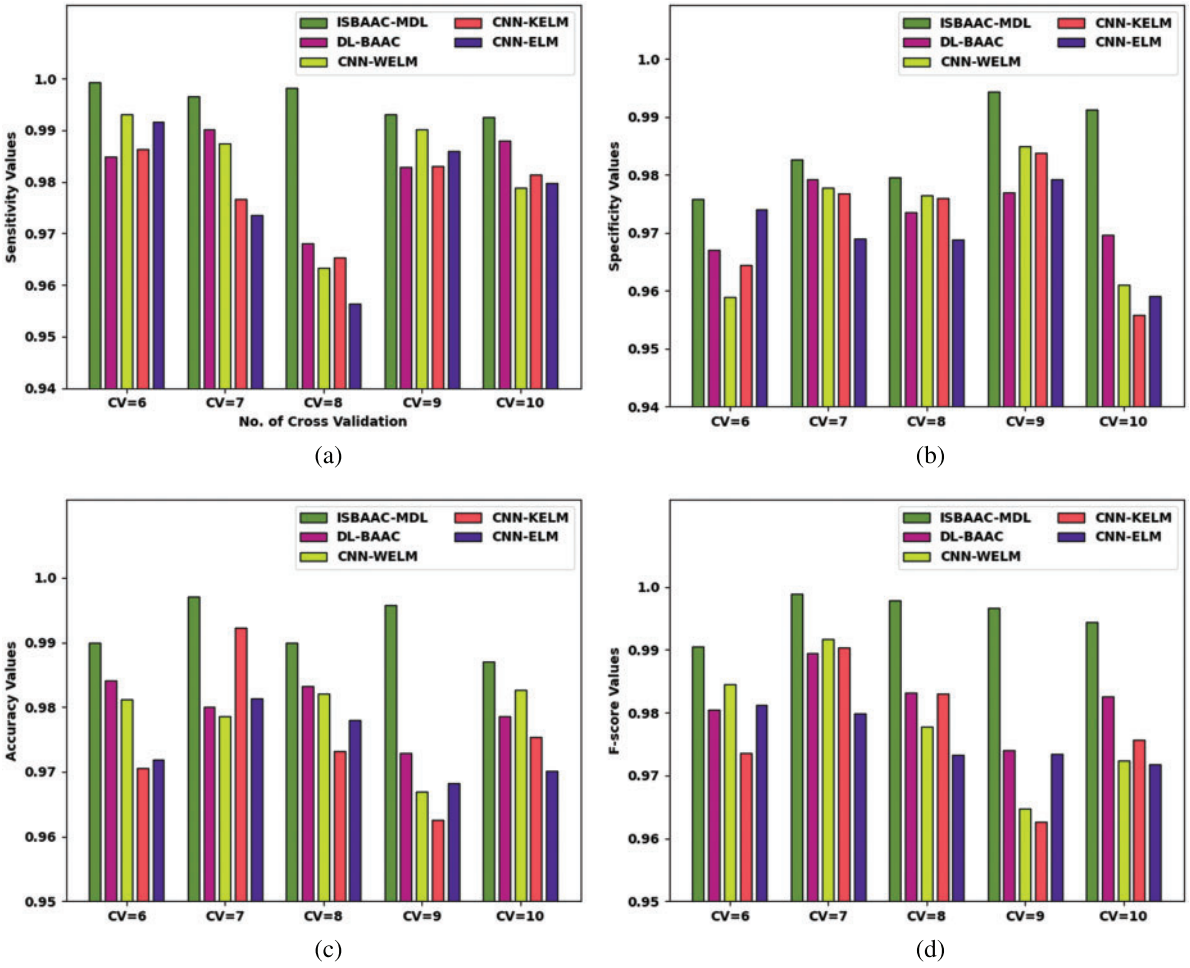


**Figure 6:** Result analysis of ISBAAC-MDL technique under distinct CV (a) $Sens_y$, (b) $Spec_y$, (c) $Accu_y$, and (d) $F_{score}$

Fig. 7 reports average classifier outcomes of the ISBAAC-MDL method with recent models. The figure inferred the enhanced performance of the ISBAAC-MDL model over other models. In relation $sens_y$, the ISBAAC-MDL model has offered raised average $sens_y$ of 0.9960 whereas the DL-BAAC, CNN-WELM, CNN-KELM, and CNN-ELM techniques have provided decreased $sens_y$ of 0.9828, 0.9826, 0.9786, and 0.9775 correspondingly. Likewise, with respect to $accu_y$, the ISBAAC-MDL model has offered increased average $accu_y$ of 0.9920 while the DL-BAAC, CNN-WELM, CNN-KELM, and CNN-ELM models have offered reduced $accu_y$ of 0.9798, 0.9783, 0.9748, and 0.9739 correspondingly. Finally, with respect to $F_{score}$, the ISBAAC-MDL algorithm has rendered increased average $F_{score}$ of 0.9956 whereas the DL-BAAC, CNN-WELM, CNN-KELM, and CNN-ELM models have provided reduced $F_{score}$ of 0.9819, 0.9782, 0.9770, and 0.9759 respectively.


**Figure 7:** Average analysis of ISBAAC-MDL technique under distinct CV (a) $Sens_y$, (b) $Spec_y$, (c) $Accu_y$, and (d) $F_{score}$

Fig. 8 highlights an extensive mean absolute error (MAE) inspection of the ISBAAC-MDL model on the bone age estimation process [28]. The figure shows that the CNN-ELM, BONet, Fine-Tuned GoogLeNet, Fine-Tuned OxfordNet, and CNN-GP models have obtained poor performance with MAE of 0.826, 0.859, 0.886, 0.892, and 0.806 respectively. Followed by, the CNN-KELM and CNN-TW3 approaches have reached slightly reduced MAE of 0.759 and 0.659 respectively. Though the DL-BAAC model has accomplished reasonable MAE of 0.348, the presented ISBAAC-MDL model has gained effectual outcome with minimal MAE of 0.311. Thus, the presented ISBAAC-MDL model has shown superior results over the other models.

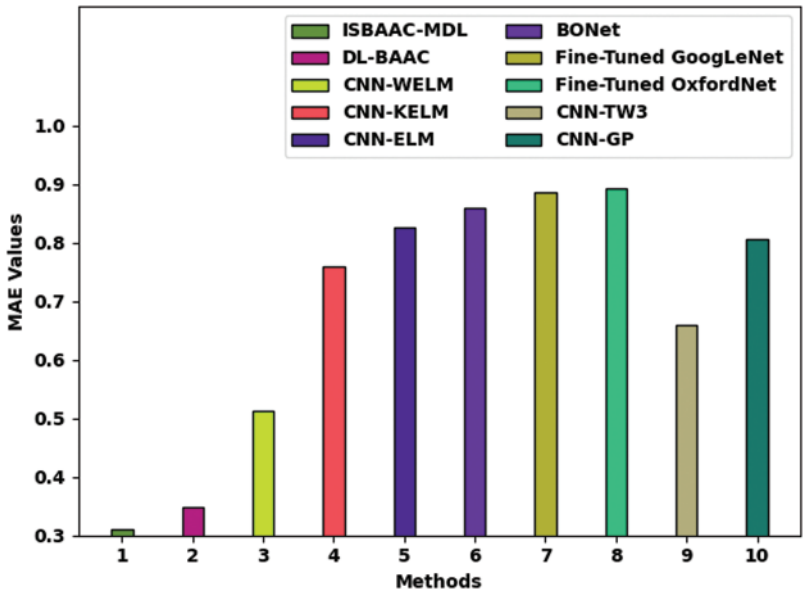


**Figure 8:** MAE analysis of ISBAAC-MDL technique with existing algorithms

## 4 Conclusion

In this article, a new ISBAAC-MDL method was advanced for the effective bone age prediction and classification process. Initially, the Mask-RCNN with MobileNet as baseline model is utilized to extract features. Then, the WOA was implemented for hyperparameter tuning of the MobileNet model. Next, the DFFM based age prediction and RBFNN based stage classification model is utilized. The experimental evaluation of the ISBAAC-MDL model is tested using benchmark dataset and the outcomes are assessed over distinct prospects. The experimental outcomes reported the better performances of the ISBAAC-MDL model over recent approaches. Thus, the ISBAAC-MDL model can be exploited for effective BAA in real time. In future, deep instance segmentation models might be involved to foster the overall efficiency of the ISBAAC-MDL model.

**Funding Statement:** Princess Nourah bint Abdulrahman University Researchers Supporting Project number (PNURSP2022R151), Princess Nourah bint Abdulrahman University, Riyadh, Saudi Arabia. The authors would like to thank the Deanship of Scientific Research at Umm Al-Qura University for supporting this work by Grant Code: (22UQU4310373DSR17).

**Conflicts of Interest:** The authors declare that they have no conflicts of interest to report regarding the present study.

## References

[1] M. W. Nadeem, H. G. Goh, A. Ali, M. Hussain, M. A. Khan *et al.,* "Bone age assessment empowered with deep learning: A survey, open research challenges and future directions," *Diagnostics*, vol. 10, no. 10, pp. 781, 2020.

[2] S. Deshmukh and A. Khaparde, "Faster region-convolutional neural network oriented feature learning with optimal trained recurrent neural network for bone age assessment for pediatrics," *Biomedical Signal Processing and Control*, vol. 71, no. 12, pp. 103016, 2022.

[3] V. I. Iglovikov, A. Rakhlin, A. A. Kalinin and A. A. Shvets, "Paediatric bone age assessment using deep convolutional neural networks," in *Int. Workshop on Deep Learning in Medical Image Analysis, Int. Workshop on Multimodal Learning for Clinical Decision Support, DLMIA 2018, ML-CDS 2018: Deep Learning in Medical Image Analysis and Multimodal Learning for Clinical Decision Support*, Lecture Notes in Computer Science book series, Springer, Cham, vol. 11045, pp. 300–308, 2018.
[4] J. H. Lee and K. G. Kim, "Applying deep learning in medical images: The case of bone age estimation," *Healthcare Informatics Research*, vol. 24, no. 1, pp. 86, 2018.
[5] S. Wang, Y. Shen, D. Zeng and Y. Hu, "Bone age assessment using convolutional neural networks," in *2018 Int. Conf. on Artificial Intelligence and Big Data (ICAIBD)*, Chengdu, China, pp. 175–178, 2018.
[6] S. Deshmukh and A. Khaparde, "Multi-objective segmentation approach for bone age assessment using parameter tuning-based U-net architecture," *Multimedia Tools and Applications*, vol. 81, no. 5, pp. 6755–6800, 2022.
[7] C. Zhao, J. Han, Y. Jia, L. Fan and F. Gou, "Versatile framework for medical image processing and analysis with application to automatic bone age assessment," *Journal of Electrical and Computer Engineering*, vol. 2018, pp. 1–13, 2018.
[8] K. Mao, W. Lu, K. Wu, J. Mao and G. Dai, "Bone age assessment method based on fine-grained image classification using multiple regions of interest," *Systems Science & Control Engineering*, vol. 10, no. 1, pp. 15–23, 2022.
[9] S. Mutasa, P. D. Chang, C. R. Shapiro and R. Ayyala, "MABAL: A novel deep-learning architecture for machine-assisted bone age labeling," *Journal of Digital Imaging*, vol. 31, no. 4, pp. 513–519, 2018.
[10] B. D. Lee and M. S. Lee, "Automated bone age assessment using artificial intelligence: The future of bone age assessment," *Korean Journal of Radiology*, vol. 22, no. 5, pp. 792, 2021.
[11] T. D. Bui, J. J. Lee and J. Shin, "Incorporated region detection and classification using deep convolutional networks for bone age assessment," *Artificial Intelligence in Medicine*, vol. 97, no. 1, pp. 1–8, 2019.
[12] S. J. Son, Y. Song, N. Kim, Y. Do, N. Kwak *et al.,* "TW3-based fully automated bone age assessment system using deep neural networks," *IEEE Access*, vol. 7, pp. 33346–33358, 2019.
[13] C. Tong, B. Liang, J. Li and Z. Zheng, "A deep automated skeletal bone age assessment model with heterogeneous features learning," *Journal of Medical Systems*, vol. 42, no. 12, pp. 249, 2018.
[14] B. Liang, Y. Zhai, C. Tong, J. Zhao, J. Li *et al.,* "A deep automated skeletal bone age assessment model via region-based convolutional neural network," *Future Generation Computer Systems*, vol. 98, no. 3, pp. 54–59, 2019.
[15] L. Su, X. Fu and Q. Hu, "Generative adversarial network based data augmentation and gender-last training strategy with application to bone age assessment," *Computer Methods and Programs in Biomedicine*, vol. 212, no. 5, pp. 106456, 2021.
[16] A. S. Almasoud, S. B. H. Hassine, F. N. A. Wesabi, M. K. Nour, A. M. Hilal *et al.,* "Automated multi-document biomedical text summarization using deep learning model," *Computers, Materials & Continua*, vol. 71, no. 3, pp. 5799–5815, 2022.
[17] R. Poonia, M. Gupta, I. Abunadi, A. Albraikan, F. Al-Wesabi *et al.,* "Intelligent diagnostic prediction and classification models for detection of kidney disease," *Healthcare*, vol. 10, no. 2, pp. 371, 2022.
[18] A. A. Malibari, R. Alshahrani, F. N. Al-Wesabi, S. B. Haj Hassine, M. A. Alkhonaini *et al.,* "Artificial intelligence based prostate cancer classification model using biomedical images," *Computers, Materials & Continua*, vol. 72, no. 2, pp. 3799–3813, 2022.
[19] A. A. Malibari, F. N. Al-Wesabi, M. Obayya, M. Alkhonaini, M. A. Hamza *et al.,* "Arithmetic optimization with Retinanet model for motor imagery classification on brain computer interface," *Journal of Healthcare Engineering*, vol. 2022, no. 1, pp. 1–11, 2022.
[20] T. Palaniswamy, "Hyperparameter optimization based deep convolution neural network model for automated bone age assessment and classification," *Displays*, vol. 73, no. 1, pp. 102206, 2022.
[21] P. N. Srinivasu, J. G. SivaSai, M. F. Ijaz, A. K. Bhoi, W. Kim *et al.,* "Classification of skin disease using deep learning neural networks with MobileNet V2 and LSTM," *Sensors*, vol. 21, no. 8, pp. 2852, 2021.

[22] K. Shankar, E. Perumal, M. Elhoseny, F. Taher, B. B. Gupta *et al.,* "Synergic deep learning for smart health diagnosis of covid-19 for connected living and smart cities," *ACM Transactions on Internet Technology*, vol. 22, no. 3, pp. 1–14, 2022.
[23] R. Gopi, P. Muthusamy, P. Suresh, C. G. G. S. Kumar, I. V. Pustokhina *et al.,* "Optimal confidential mechanisms in smart city healthcare," *Computers, Materials & Continua*, vol. 70, no. 3, pp. 4883–4896, 2022.
[24] D. A. Pustokhin, I. V. Pustokhina, P. Rani, V. Kansal, M. Elhoseny *et al.,* "Optimal deep learning approaches and healthcare big data analytics for mobile networks toward 5G," *Computers & Electrical Engineering*, vol. 95, no. 11, pp. 1–14, 2021.
[25] S. Chakraborty, A. K. Saha, S. Sharma, S. Mirjalili and R. Chakraborty, "A novel enhanced whale optimization algorithm for global optimization," *Computers & Industrial Engineering*, vol. 153, no. 5, pp. 107086, 2021.
[26] R. Atefinia and M. Ahmadi, "Network intrusion detection using multi-architectural modular deep neural network," *The Journal of Supercomputing*, vol. 77, no. 4, pp. 3571–3593, 2021.
[27] C. She, Z. Wang, F. Sun, P. Liu and L. Zhang, "Battery aging assessment for real-world electric buses based on incremental capacity analysis and radial basis function neural network," *IEEE Transactions on Industrial Informatics*, vol. 16, no. 5, pp. 3345–3354, 2020.
[28] C. Spampinato, S. Palazzo, D. Giordano, M. Aldinucci and R. Leonardi, "Deep learning for automated skeletal bone age assessment in X-ray images," *Medical Image Analysis*, vol. 36, pp. 41–51, 2017.